Global observables in the PHENIX experiment

D. Silvermyr for the PHENIX Collaboration

Department of Physics, Lund University,
Box 118, 221 00 Lund, Sweden

Abstract

The Relativistic Heavy Ion Collider (RHIC) has made it possible to study hadronic matter under unprecedented conditions in terms of temperature and energy density. Global variables are essential for the characterization of nuclear collisions at ultra-relativistic energies. The PHENIX experiment has several detectors which provide information about the global properties and hence the initial conditions, such as energy density, reached in these collisions. The results discussed here are charged particle multiplicity, transverse energy, net charge fluctuations and fluctuations in mean p_T.

1 Introduction

The PHENIX experiment[1] has been designed to measure a broad variety of signals from A-A and (polarized) p-p collisions at RHIC. PHENIX aims to study both lepton, photon and hadron observables, i.e. both penetrating probes generated in the early stages of the collision, complemented with information on the hadronization process. The data presented here are mainly from Au+Au collisions at $\sqrt{s_{NN}} = 130$ GeV, measured in the two central arms, each covering $90°$ in azimuth, and with $|\eta| < 0.35$.

The central arms contain three tracking sub-systems: Drift Chambers (DC), Pad Chambers (PC) and Time Expansion Chambers (TEC). There are two types of Electromagnetic Calorimeters (EMCal) in the central arms, one made of lead-glass (PbGl) and the other made of lead and scintillator material (PbSc). For charged-particle identification there is also a Time-of-Flight system (TOF) and Ring Imaging Cherenkov counters (RICH). These sub-systems, together with start-time information from a set of Beam-Beam Counters (BBC), located in the region $3 < |\eta| < 3.9$ at ± 1.44 m from the center of the interaction region, identify hadrons and electrons over a broad range of transverse momentum.

Minimum bias triggers were formed using coincidences between the Beam-Beam Counters and between the RHIC-standard Zero-Degree Calorimeters (ZDCs), which detect neutral particles emitted along the beam.

2 Charged Particle Multiplicity

The main sub-systems utilized in this analysis, using data obtained with the magnetic field off, were the Pad Chambers (PC) in the central tracking arms, the Beam-Beam Counters (BBC), and the Zero-Degree Calorimeters (ZDCs). PC is used for track reconstruction while BBC and ZDC were used for triggering and centrality selection. All three systems provide complementary information on the position of the collision vertex.

The track reconstruction is done by combining all hits from the layers of Pad Chambers at 2.5 and 5 m distance from the beam (PC1 and PC3 respectively). The straight line obtained by combining every hit in PC3 to every hit in PC1 defines a track if its intersection point with a plane through the beam line lies within a circular window of radius R from the vertex position. A rather large R cut of 25 cm was used to minimize losses of real tracks. The best available vertex position is used: the first choice is always the vertex derived from PC1/3, which is determined from the distribution of the intersection points along the beam direction. For low multiplicity events, where the number of tracks is too small to allow a PC vertex determination, the best choice is the vertex position from the time-difference measured by BBC.

Inherent to the procedure is a combinatorial background contribution, which however can be reliably determined, on the average, by using a technique where each PC1 sector is interchanged with its neighbor. The number of real tracks is then obtained by subtracting the average combinatorial background from the total number of tracks. The analysis method and results from the first run at $\sqrt{s_{NN}} = 130$ GeV are described in detail in ref. [2]. The result for the 5% most central collisions is $dN_{ch}/d\eta = 622 \pm 41$, corresponding to a $dN_{ch}/d\eta$ per participant pair of 3.58 ± 0.26.

Several measurements of dN_{ch}/dy and $dN_{ch}/d\eta$ at midrapidity have been carried out by various experiments at different energies. The results of some of these are compiled in Fig. 1a. The figure incorporates results for the central unit of rapidity from fixed-target heavy-ion experiments at AGS[3], SPS[4, 5], and recent results from RHIC[2, 6]. Data from p-p experiments at the ISR, SPS and the Tevatron[7] are also included. The p-p and A-A data show similar trends: approximately logarithmic increase or weak power law dependencies on $\sqrt{s_{NN}}$, although with different coefficients.

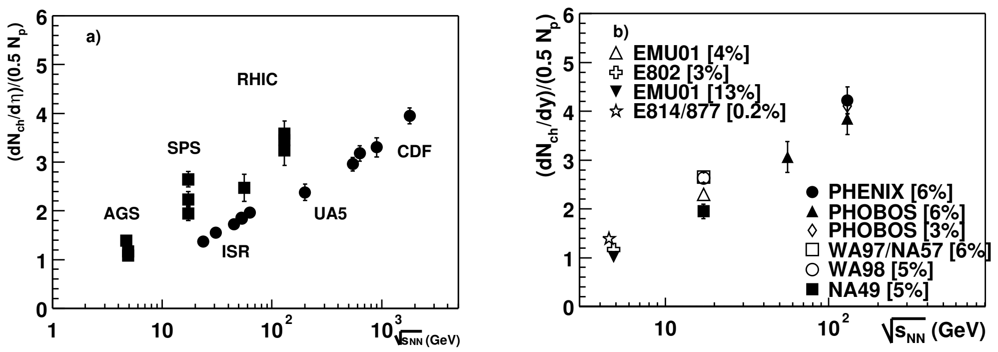

Figure 1: (a) Pseudorapidity density, $dN_{ch}/d\eta$, per participant pair: A-A and p-p data. (b) Rapidity density, dN_{ch}/dy, per participant pair: A-A data.

To be able to make a relevant comparison of the fixed-target and collider data, the RHIC points need to be scaled to dN_{ch}/dy since $dN_{ch}/d\eta$ is only a good approximation to dN_{ch}/dy at fixed-target. The obtained scaling factors between $dN_{ch}/d\eta$ and dN_{ch}/dy are somewhat model dependent. According to HIJING[8], the scaling factors at RHIC at 56 and 130 GeV were roughly 1.2.

An approximately logarithmic scaling of the A-A rapidity density values at midrapidity with $\sqrt{s_{NN}}$ is observed in Fig. 1b. To further investigate the nature of the scaling, two different functional forms: $A + B \cdot ln(s)$, logarithmic increase with s, and $Y \cdot s^X$, power law behavior, previously used to fit p-p data, were fitted to the values of dN_{ch}/dy per participant pair.

The PHOBOS result at 200 GeV[9] of 3.78 $\pm$ 0.25 for $dN_{ch}/d\eta$ per participant pair, corresponds to an increase from 130 GeV by a factor of 1.14 $\pm$ 0.05, while BRAHMS observe a factor of 1.14 $\pm$ 0.01[10]. Preliminary results from PHENIX give an increase in the same quantity by a factor of 1.15 $\pm$ 0.04.

The points were scaled with the same factor as for 130 GeV to account for the difference between $dN_{ch}/d\eta$ and dN_{ch}/dy at 200 GeV. The average at 200 GeV is in good agreement with the logarithmic scaling fit. To summarize, the dN_{ch}/dy values for the A-A data studied so far, are well described by logarithmic scaling with the center-of-mass energy.

Logarithmic scaling predicts an increase of roughly 80% in dN_{ch}/dy per participant pair to LHC energies, $\sqrt{s_{NN}}$ = 5 500 GeV, from 130 GeV, while the power law behaviour implies an increase of about 300%. The total charged-particle multiplicity will increase with an additional factor due to the widened rapidity region of the produced particles. From ref. [11], reporting a total charged-particle multiplicity of 4 200 at 130 GeV, the equivalent quantity at

LHC can be estimated to be about 13 000, assuming logarithmic scaling. If instead the power law fit describes the data, which cannot be excluded by the present analysis, due to the uncertainties in the data points at the SPS and RHIC, the total charged-particle multiplicity will be about 30 000 at LHC.

3 Transverse Energy

The transverse energy (E_T) is defined as:

$$E_T = \sum_i E_i \sin\theta_i \tag{1}$$

where θ is the polar angle, and E_i is by convention taken as the kinetic energy for nucleons and the total energy for all other particles[12], and the sum is taken over all particles emitted into the acceptance for each event. E_T measurements, even in limited apertures at mid-rapidity, provide excellent characterization of the nuclear geometry of a reaction on an event-by-event basis and are sensitive to the underlying reaction dynamics[13].

The transverse energy was measured using the PbSc EMCal[14] in a fiducial aperture $|\eta| \leq 0.38$ in pseudorapidity and $\Delta\phi = 44.4^\circ$ in azimuth. E_T was computed for each event (Eq. 1) using clusters of energy greater than 20 MeV. The angle θ_i is computed from the centroid of the cluster of energy E_i assuming a particle originating from the event vertex. The data sample was collected with the magnetic field off. The full analysis, including the determination of the in-flow contribution and losses, and results from the first run at $\sqrt{s_{NN}} = 130$ GeV are described in detail in ref. [15].

Figure 2a shows that $\langle dE_T/d\eta|_{\eta=0}\rangle$ per participant increases with $N_{\rm part}$, closely paralleling the rise in charged particle density. This is better illustrated in Fig. 2b where the ratio $\langle dE_T/d\eta|_{\eta=0}\rangle/\langle dN_{ch}/d\eta|_{\eta=0}\rangle$ remains constant at a value of ~ 0.8 GeV, independent of centrality. The WA98 data[4] for mid-rapidity $\langle dE_T/d\eta|_{\rm mid}\rangle$ per participant are shown in Fig. 2a and are essentially independent of $N_{\rm part}$ for $N_{\rm part} > 200$. WA98 parameterizes their data as $dE_T/d\eta|_{\rm mid} \propto N_{\rm part}^{\alpha}$ with $\alpha = 1.08 \pm 0.06$ while the same parameterization for our data yields $\alpha = 1.13 \pm 0.05$. Fig. 2 also shows that $\langle dE_T/d\eta|_{\eta=0}\rangle$ for central Au+Au collisions at $\sqrt{s_{_{NN}}} = 130$ GeV is about 40% larger than found by WA98. As discussed in the previous section, a comparison between fixed-target and collider experiments is more appropriate in the rapidity variable and the correction to the energy density $dE_T/dy|_{y=0}$, yields another 20%. For both energies, the ratio $\langle dE_T/d\eta\rangle/\langle dN_{ch}/d\eta\rangle$ remains constant versus centrality at roughly the same value, ~ 0.8 GeV (Fig. 2b).

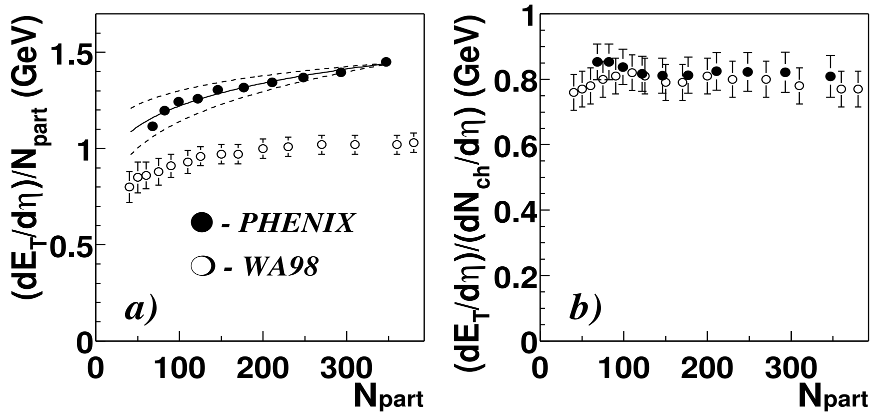

Figure 2: (a) PHENIX transverse energy density per participant $dE_T/d\eta|_{\eta=0}/N_{\text{part}}$ for Au+Au collisions at $\sqrt{s_{_{NN}}} = 130$ GeV as a function of N_{part}, compared to data from WA98[4] for Pb+Pb collisions at $\sqrt{s_{_{NN}}} = 17.2$ GeV. (b) PHENIX $dE_T/d\eta|_{\eta=0}/dN_{ch}/d\eta|_{\eta=0}$ versus N_{part}, including all systematic errors, compared to WA98. Note that the WA98 data in both (a) and (b) have an additional $\pm 20\%$ overall systematic error which is not shown.

In conclusion, the mid-rapidity transverse energy density for central Au+Au collisions is at least 1.6 times larger at $\sqrt{s_{_{NN}}} = 130$ GeV (RHIC) than at $\sqrt{s_{_{NN}}} = 17.2$ GeV (SPS). The variation of the E_T density per participant with centrality is very similar to the previously reported dependence of charged multiplicity density per participant at RHIC energies. These results, together with the observed constancy of $\langle E_T \rangle / \langle N_{ch} \rangle$ at a value ~ 0.8 GeV, indicate that the additional energy density at RHIC energies is achieved mainly by an increase in particle production rather than by an increase in transverse energy per particle. The results are not inconsistent with the observed minor increase in the the average transverse momentum.

4 Net Charge Fluctuations

Recent theoretical investigations[16, 17, 18] predict a drastic decrease of the event-by-event fluctuations of the net charge, $Q = n_+ - n_-$ in local phase-space regions as a signature of the plasma state. The main concern of the theoretical discussions is how and why the original distribution survives the transition back to ordinary matter[19, 20].

The data sample used in this analysis consists of a total of about 5×10^5 minimum bias events. The combination of reconstructed DC tracks with matching hits in the innermost Pad Chamber plane (PC1) defines the sign of the charge

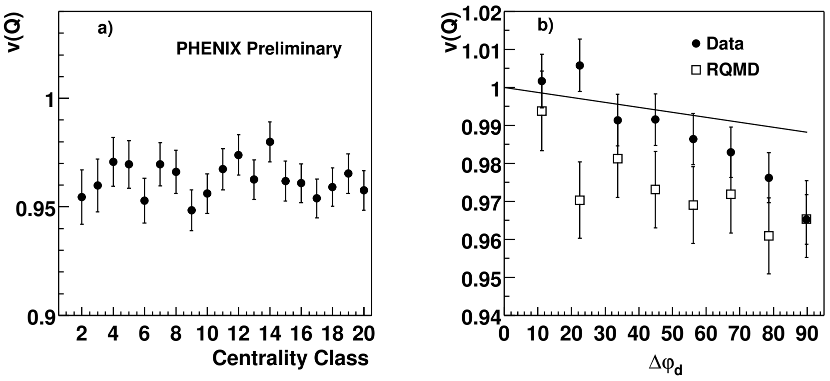

Figure 3: (a) Normalized variance $v(Q)$ as a function of centrality class. (b) $v(Q)$ as a function of how large part of the azimuthal acceptance that is used, for the 10 % most central events in data and RQMD. The solid line shows the expectation from global charge conservation.

of the particle and also provides a high resolution measurement of the transverse momentum, p_T, of tracks originating from the collision vertex.

In each event the numbers of positively charged particles, n_+, negatively charged particles, n_-, and their sum, n_{ch}, are recorded. In a stochastic scenario with a fixed number of charged particles within the acceptance, where each particle is assigned a random charge (+1 or −1 with the same probability), the variance of the net charge, Q, is

$$V(Q) \equiv \langle Q^2 \rangle - \langle Q \rangle^2 = n_{ch}. \tag{2}$$

The normalized variance in Q is $v(Q) \equiv V(Q)/n_{ch}$.

The event sample was divided into 20 centrality classes, each containing 5 % of the total number of events. Class 20 corresponds to the most central events. Fig. 3a shows the $v(Q)$ results for the different centrality classes. The values are consistently below unity and show no statistically significant centrality dependence. In a stochastic scenario, a reduction in $v(Q)$ is expected from global charge conservation, $v(Q) = (1 - p)$, where p is the fraction of charged particles that are observed. The fraction p can be varied in the analysis by selecting tracks from parts of the detector. The azimuthal coverage of the tracking arm is 90°, and Fig. 3b shows the $v(Q)$ result when the analysis is restricted to tracks within an azimuthal interval $\Delta\varphi_d$. The data are found to agree well with predictions from the RQMD model[21].

Further reduction beyond global charge conservation is expected from resonance decays. For a hadron gas, one expects a reduction to $v(Q) \simeq 0.7(1 - p)$.

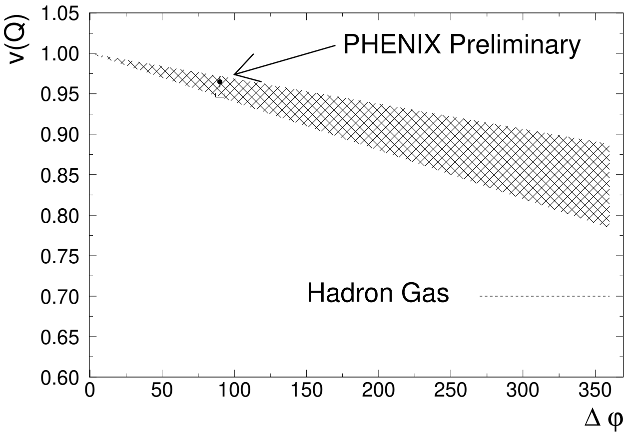

Figure 4: The preliminary result for the net charge fluctuations for the 10 % most central events, extrapolated to full azimuthal coverage.

The prediction for a QGP is much lower: $v(Q) \simeq 0.25(1-p)$[16]. The preliminary result for the net charge fluctuations in the region -0.35 $< \eta <$ 0.35, $p_T >$ 200 MeV/c, $\Delta\varphi = \pi/2$,

$$v(Q) = 0.965 \pm 0.007(stat.) - 0.019(syst.) \tag{3}$$

is obtained for the 10 % most central events. A linear extrapolation of this value to full azimuthal coverage, following the trend seen in Fig. 3b, gives a value of $v(Q)$ in the range 0.78 - 0.86, in qualitative agreement with calculations from a hadronic gas. This is illustrated in Fig. 4.

5 Event-by-event fluctuations in Mean p_T

Phase instabilities near the QCD phase transition can result in non-statistical fluctuations that are detectable in final state observables[22], e.g a broadening of the transverse momentum or transverse energy distributions of produced particles for different classes of events. This phenomenon is expected to be detected experimentally by searching for deviations of the distributions of the event-by-event mean transverse momentum M_{p_T} or mean transverse energy M_{e_T} of produced particles from the random distributions expected for statistically independent particle emission. The presentation here is focused on M_{p_T}.

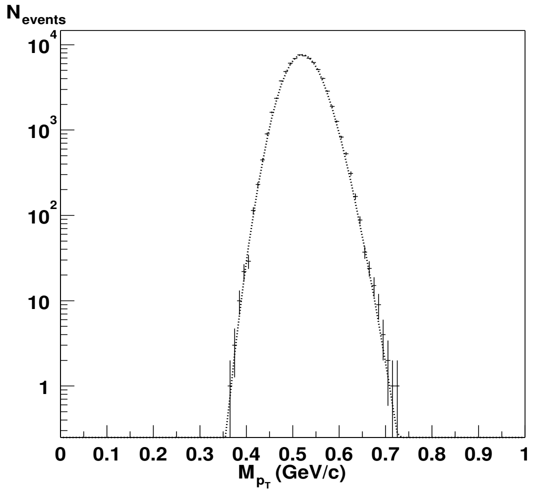

Figure 5: The preliminary M_{p_T} distribution for the 0-5% centrality class. The curve is the result of a Γ distribution calculation with parameters taken from the semi-inclusive p_T spectra.

The transverse momentum of charged particles traversing the PHENIX acceptance is measured by DC and PC1. The fiducial volume of the M_{p_T} analysis spans an azimuthal range of $\Delta\phi = 58.5°$ and covers the pseudorapidity range $|\eta| < 0.35$. Reconstructed tracks are required to contain a match to a hit in PC1 to insure that the tracks are well reconstructed in three dimensions for reliable momentum determination.

In order to compare the M_{p_T} distributions to what is expected for statistically independent particle emission, mixed events are considered as the baseline for the random distribution. To compare directly the semi-inclusive p_T distribution to the M_{p_T} distribution assuming statistically independent particle emission, the closed form prescription outlined in ref. [23] is used. Overlayed on the data as a dotted curve in Fig. 5, is the calculation following that prescription. The agreement between the data and the calculation illustrates the absence of large non-statistical fluctuations in the data.

To quantify the magnitude of the deviation of fluctuations from the expectation of statistically independent particle emission, the magnitude of the fluctuation ω in M_{p_T}, is defined as

$$\omega = \frac{(< M_{p_T}^2 > - < M_{p_T} >^2)^{1/2}}{< M_{p_T} >} = \frac{\sigma_{M_{p_T}}}{< M_{p_T} >}. \tag{4}$$

Centrality class	ω_{data} (%)	F (%)
0 - 5 %	7.37 $\pm$ 0.10	1.9 $\pm$ 2.1
0 - 10 %	7.85 $\pm$ 0.13	2.0 $\pm$ 2.5
10 - 20 %	9.52 $\pm$ 0.14	2.1 $\pm$ 2.2
20 - 30 %	11.7 $\pm$ 0.21	1.8 $\pm$ 3.0

Table 1: The preliminary fluctuation quantities for the M_{p_T} analysis.

Here, the magnitude of any excess fluctuations will be quoted as the fraction of the fluctuation which is not due to statistically independent particle emission as given by

$$F = \frac{(\omega_{data} - \omega_{baseline})}{\omega_{baseline}} = \frac{(\sigma_{data} - \sigma_{baseline})}{\sigma_{baseline}}. \tag{5}$$

For the M_{p_T} distributions, the data and mixed event distributions are indistinguishable. The preliminary results for the M_{p_T} fluctuations are summarized in Table 1. The fluctuations in the M_{p_T} distributions for all centrality classes are consistent with the presence of no fluctuations in excess of the random expectation. The magnitude of F in all cases is positive, which may be due to the presence of Hanbury-Brown-Twiss correlations.

References

[1] PHENIX Collaboration, D. P. Morrison *et al.*, Nucl. Phys. A **638** (1998) 565.

[2] PHENIX Collaboration, K. Adcox *et al.*, Phys. Rev. Lett. **86** (2001) 3500.

[3] EMU01 Collaboration, M. I. Adamovich *et al.*Phys. Lett. B **322** (1994) 166; E802 Collaboration, L. Ahle *et al.*, Phys. Rev. C **59** (1999) 2996; E877 Collaboration, J. Barrette *et al.*, Phys. Rev. C **51** (1995) 3309.

[4] WA98 Collaboration, M. M. Aggarwal, *et al.*, Eur. Phys J. **C18**, 651 (2001).

[5] EMU01 Collaboration, M. I. Adamovich *et al.*, Phys. Lett. B **407** (1997) 92; NA49 Collaboration, J. Bächler *et al.*, Nucl. Phys. A **661** (1999) 45; WA97/NA57 Collaborations, F. Antinori *et al.*, Eur. Phys. J. C **18** (2000) 57.

[6] PHOBOS Collaboration, B. B. Back *et al.*, Phys. Rev. Lett. **85** (2000) 3100, nucl-ex/0105011.

[7] W. Thome *et al.*, Nucl. Phys. B **129** (1977) 365; UA5 Collaboration, G. J. Alner *et al.*, Z. Phys. C **33** (1986) 1; CDF Collaboration, F. Abe *et al.*, Phys. Rev. D **41** (1990) 2330.

[8] X. N. Wang and M. Gyulassy, Phys. Rev. **D44**, 3501 (1991), version 1.35.

[9] PHOBOS Collaboration, B. B. Back *et al.*, nucl-ex/0108009.

[10] BRAHMS Collaboration, I. G. Bearden *et al.*, nucl-ex/0112001.

[11] PHOBOS Collaboration, B. B. Back *et al.*, nucl-ex/0106006.

[12] Helios Collaboration, T. Åkesson, *et al.*, Z. Phys. **C38**, 383, 397 (1988).

[13] e.g. see *Proc. Quark Matter 1984*, ed. K. Kajantie (Springer, Berlin 1985); *Proc. Quark Matter 1987*, eds. H. Satz, H. J. Specht, R. Stock, Z. Phys. **C38**, 1-370 (1988).

[14] E. Kistenev et.al., *Proc. 5th Int. Conf. on Calorimetry in HEP*, World Scientific (1994), pp. 211-223; G. David *et al.*, IEEE Trans. Nucl. Sci. **45**, 692, 705 (1998).

[15] PHENIX Collaboration, K. Adcox *et al.*, Phys. Rev. Lett. **87** (2001) 052301.

[16] S. Jeon and V. Koch, Phys. Rev. Lett. **85**, 2076 (2000); M. Bleicher, S. Jeon and V. Koch, Phys. Rev. **C62**, 061902(R) (2000).

[17] M. Asakawa, U. Heinz and B Müller, Phys. Rev. Lett. **85**, 2072 (2000).

[18] H. Heiselberg and A. D. Jackson, Phys. Rev. **C63**, 064904 (2001).

[19] E. V. Shuryak and M. A. Stephanov, Phys.Rev. **C63**, 064903 (2001).

[20] K. Fialkowski and R. Wit, Europhys. Lett. **55** (2), 184 (2001).

[21] H. Sorge, Phys. Rev. **C 52** 3291 (1995).

[22] H. Heiselberg, Phys. Repts. **351**, 161 (2001).

[23] M. J. Tannenbaum, Phys. Lett. **B498**, 29 (2001).